J. Fluid Mech. (1995), *vol.* 304, *pp.* 143–159

Directional solidification into static stability

By KIRK BRATTKUS

Department of Mathematics, Southern Methodist University, Dallas, TX 75275-0156, USA

(Received 26 September 1994 and in revised form 22 February)

Consider the directional solidification of a binary alloy rejecting a heavy solute as it solidifies upward. If the solidification front is planar, the fluid melt ahead of the front is stably stratified and convection is not expected. In this paper we analyse the linear stability of planar solidification asymptotically in the limit of large solutal Rayleigh number, R. Three distinct linear modes are found which correspond to internal waves, buoyancy edge waves, or morphological modes. Of these three modes, only the morphological modes are subject to an instability. We find that for large Rayleigh number this instability first occurs at long wavelengths with wavenumbers that scale on $R^{-1/14}$. The scalings derived from the linear analysis are used to construct a nonlinear theory for the morphological instability in the large Rayleigh number limit. Similarity solutions are found which describe steadily convecting, non-planar growth reminiscent of an observed phenomenon known as steepling.

1. Introduction

The flow of a liquid melt can significantly alter the stability of solidification fronts and the subsequent development of microstructure (Glicksman, Coriell & McFadden 1986; Davis 1990). This is important since flow is present during most of the solidification that occurs on Earth: as lakes of magma cool, as casts of molten aluminium freeze into ingots, or as crystals of doped semiconductor are pulled from the melt. The principal source of the flow is a buoyant convection driven by rejected impurities whose distributions depend sensitively on the morphology of the solidification front. Although solidification from a convecting melt is the rule rather than the exception, theoretical work on the coupled problem is largely undeveloped.

The control and elimination of convection is important to crystal growers producing uniform single crystals of material for electronic-device applications. It is believed that convection is primarily responsible for dopant striations that degrade the quality of a crystal. One way of removing the convection is to orient a planar solidification front that rejects a heavy solute so that growth is in the upward direction. The liquid melt in this case is stably stratified with the denser liquid lying close to the interface. As long as the front remains planar the fluid is statically stable to convection.

However, the solidification front is deformable and it may not remain flat. The directional solidification experiments of Burden, Hebditch & Hunt (1973) on metal alloys and later those of Verhoeven, Mason & Trivedi (1986) clearly show that convection may occur during upward growth and that this convection is accompanied by non-planar solidification fronts. The non-planar fronts always bend backwards and are observed to disappear as the solutal Rayleigh number is decreased, either by increasing the pulling velocity V or by decreasing the equilibrium solute concentration C_∞. The scale of the curvature in the front is the same as the container size, hundreds of times

larger than the typical microstructural scale. These macroscopically curved fronts appear in experiments with solutal Rayleigh numbers that are typically larger than 10^6.

Burden *at al.* (1973) qualitatively interpret this 'steepling' effect as an instability of planar growth. They suggest that when planar interfaces curve slightly backward, horizontal solute gradients produce a convective flow that washes heavy solute away from peaks in the interface. The added solute along the sloping sides of the front reduces the equilibrium temperature and tends to melt the front further back, increasing its curvature. Although this mechanism is plausible, the argument does not predict the scale of the deflection. Moreover, it does not explain why planar solidification is ever observed!

Coriell & McFadden (1989) have interpreted steepling as an aspect of the morphological instability (for a review of the morphological instability see Coriell & McFadden 1993). They consider the linear stability of upward planar directional solidification for a mixture with heavy solute but include the effects of both thermal and solutal buoyancy. When the solutal Rayleigh number R is set to zero, they find that the morphological instability is dramatically altered by the presence of thermal buoyancy. If the thermal Rayleigh number is 'switched on', i.e. if the acceleration due to gravity is changed from $0g$ to $1g$, critical solute concentrations may decrease by three orders of magnitude while the critical wavenumber may decrease by more than two. Horizontal temperature gradients create a convection that transports solute toward the interface in a way which is cooperative with the mechanism producing a morphological instability and the length scales of the instability move toward the length scales of thermal convection.

Coriell & McFadden (1989) determine that for parameters relevant to experiments, the length scale of the instability becomes comparable to the size of the experimental container suggesting that the observed steepling may be related to a morphological instability. In a sense, the macroscopic deflection of the interface results from a microscopic instability (the morphological instability) modified by convection.

They also find that incorporating solute buoyancy is stabilizing. As the solutal Rayleigh number is increased from zero, the critical wavenumber remains small while the critical concentration increases. If the Coriell–McFadden picture is an accurate description of steepling, it is essentially governed by thermal convection and is not due to the mechanism of solutal buoyancy as Burden *et al.* (1973) suggest.

In this article we reconsider the upward directional solidification of a dilute binary alloy rejecting a heavy solute. We include the effects of solute buoyancy but exclude thermal buoyancy. We begin by considering the linear stability of planar directional solidification in the limit of large solutal Rayleigh number. We discover three distinct classes of linear modes. Two of these classes are essentially convective modes with small interface deflection. They represent either internal waves which propagate throughout the bulk fluid or buoyancy edge waves that remain trapped in a thin layer near the interface. All of these modes are stable. The last mode has significant interface deformation and represents the Mullins–Sekerka mode (Mullins & Sekerka 1964) for large solutal Rayleigh numbers. This mode is unstable when the equilibrium concentration C_∞ is sufficiently large. Linear theory reveals that the critical wavenumber scales on $R^{-1/14}$ for large R so that the morphological instability occurs at long wavelengths *even in the absence of thermal buoyancy*. We find that solute buoyancy preferentially destabilizes small-wavenumber disturbances and produces the trend toward long waves.

Long-wavelength instabilities naturally lead to nonlinear evolution equations governing transition. There are now several recognized long-wave regimes for directional

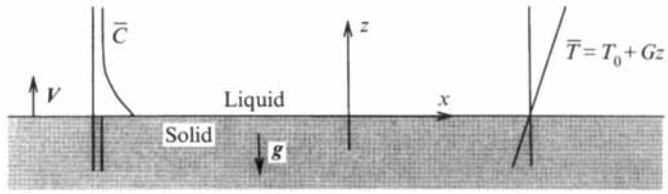

FIGURE 1. Schematic of a planar directional solidification front pulled at a constant velocity V through a linear temperature field, $\bar{T}$. The melt is static and the rejected solute establishes an exponential profile, $\bar{C}$. Because the solute is heavy and the acceleration due to gravity $\boldsymbol{g}$ acts downward, the quiescent melt is statically stable.

solidification with and without melt flow (Riley & Davis 1990). The existence of a long-wave evolution equation allows for important progress to be made on the nonlinear description of the morphological instability. For example, it is significantly easier to derive weakly nonlinear theories from an evolution equation than from the original model. Questions of pattern selection are also much easier to address. Also, problems that may not be numerically tractable can be investigated in the long-wave regime through numerical simulations of the evolution equation.

We use the long-wave regime for upward directional solidification at large solutal Rayleigh numbers to develop an asymptotic theory which can be further reduced to an evolution equation for the shape of the interface. In the last section of this article we employ the long-wave theory to find a set of similarity solutions for steady, non-planar solidification fronts which may have some relevance to the observations of steepling.

2. Equations of motion

In this section we outline our model of buoyant directional solidification and refer to earlier papers (Coriell *et al.* 1980; Hurle, Jakeman & Wheeler 1982) for a description of more complete models. The directional solidification of a binary mixture, pulled at a velocity $V\hat{\boldsymbol{k}}$ through a temperature field fixed to the laboratory frame of reference, is sketched in figure 1. At a temperature close to the melting temperature of a pure material, T_M, the binary mixture is continuously solidified at a rate V. The equilibrium temperature of the planar solid–liquid interface is $T_0 = T_M + mC_0$ where m is the slope of the liquidus line and C_0 is the concentration of solute at the interface. We adopt the frozen-temperature approximation (Langer 1980) and assume that the temperature field $\bar{T}$ is linear with constant gradient G, independent of the solidification.

As material freezes, solute is typically rejected at the solidification front. When the equilibrium concentration C_∞ is small, the ratio of solute concentrations across the solid–liquid interface is a constant k. Although it is essentially immobile once frozen into the alloy, the solute diffuses freely in the liquid phase with diffusivity $\mathscr{D}$. If the solidification front is planar and if the liquid melt remains motionless, the rejected solute establishes a diffusive boundary layer of thickness $\mathscr{D}/V$.

We assume that the solute is heavier than the surrounding solvent and that the density of the mixture is related to the solute concentration through a linearized equation of state,

$$(\rho - \rho_\infty)/\rho_\infty = \beta(C - C_\infty). \tag{2.1}$$

Here ρ_∞ is the equilibrium density of the mixture, $\beta > 0$ is the coefficient of solute expansion, and we have assumed that the liquid density is independent of temperature.

When the directional solidification cell is oriented so that growth is in the upward direction, the density stratification produced by the layer of rejected solute is statically stable.

The two-dimensional Boussinesq equations governing the dimensionless stream function $\psi(x,z,t)$ and the dimensionless solute concentration $c(x,z,t)$ in a frame of reference moving with the solidification front at a constant velocity V may be written as follows:

$$\left.\begin{aligned} S^{-1}[(\partial/\partial t - \partial/\partial z)\nabla^2\psi + J(\psi,\nabla^2\psi)] &= \nabla^4\psi - R\partial c/\partial x, \\ (\partial/\partial t - \partial/\partial z)c + J(\psi,c) &= \nabla^2 c, \end{aligned}\right\} \tag{2.2}$$

where $J(u,v)$ is a shorthand notation for $\det[\partial(u,v)/\partial(x,z)]$. Here the stream function which measures velocity in the laboratory frame has been scaled on the diffusivity $\mathscr{D}$ while c represents the difference between the dimensional concentration and C_∞ scaled by the miscibility gap $\Delta C = (1-k)C_\infty/k$. Lengths have been scaled by $\mathscr{D}/V$ and time has been scaled by $\mathscr{D}/V^2$. The non-dimensional groupings that appear involve the liquid viscosity ν; they are the Schmidt number $S = \nu/\mathscr{D}$ and the solutal Rayleigh number

$$R = \frac{g\beta\Delta C(\mathscr{D}/V)^3}{\nu\mathscr{D}}. \tag{2.3}$$

At the solid–liquid interface $z = h(x,t)$, with outward-pointing unit normal $\hat{\boldsymbol{n}}$, normal velocity v_n, and curvature κ, we apply a condition of no slip,

$$\psi = \nabla\psi \cdot \hat{\boldsymbol{n}} = 0, \tag{2.4}$$

a condition of solute conservation,

$$\nabla c \cdot \hat{\boldsymbol{n}} + [k + (1-k)c]v_n = 0, \tag{2.5}$$

and the Gibbs–Thomson condition of thermodynamic equilibrium,

$$c = 1 - M^{-1}h - \Gamma\kappa. \tag{2.6}$$

The remaining non-dimensional parameters Γ and M measure temperature changes along the solid–liquid interface. The first parameter, $\Gamma = \tilde{\Gamma}V/m\Delta C\mathscr{D}$, is proportional to $\tilde{\Gamma}$, the amount that the equilibrium temperature of a spherical seed with unit radius is reduced by surface energy. $\tilde{\Gamma}$ is typically on the order of 10^{-5}K cm. The second parameter, $M = m\Delta CV/\mathscr{D}G$, is a morphological number inversely proportional to the gradient of the external temperature field.

A basic-state solution to the governing system represents planar directional solidification into a quiescent melt. The solute concentration in this case is exponential and the stream function is identically zero,

$$\bar{c} = \mathrm{e}^{-z}, \quad \bar{\psi} = 0, \quad \bar{h} = 0. \tag{2.7}$$

In the next section we examine whether this planar convectionless growth is linearly stable.

3. Linear theory: $R \gg 1$

The evolution of small variations from steady, planar growth with no convection is governed by the linearized disturbance equations obtained by linearizing the equations of motion (2.2),(2.4)–(2.6) about the basic-state solution (2.7). If we assume that these variations can be decomposed into a superposition of normal modes,

$[C(z), \Psi(z), H]e^{iqx+\sigma t}$, then the evolution of the disturbance is prescribed by a linear growth rate σ that satisfies the characteristic equation. If differentiation with respect to the vertical coordinate z is denoted by D, the linearized disturbance equations result in the following eigenvalue problem for the normal modes:

$$\left.\begin{aligned}[(\mathrm{D}^2 - q^2)^2 + S^{-1}(\mathrm{D}^2 - q^2)(\mathrm{D} - \sigma)]\Psi - iqRC = 0,\\ iqe^{-z}\Psi + (\mathrm{D}^2 + \mathrm{D} - \sigma - q^2)C = 0,\end{aligned}\right\} \tag{3.1}$$

on $0 \leqslant z < \infty$ subject to the boundary conditions at $z = 0$,

$$\left.\begin{aligned}\Psi = \mathrm{D}\Psi = 0,\\ \mathrm{D}C + [1 - k + (\sigma + k)(1 - M^{-1} - q^2\Gamma)^{-1}]C = 0.\end{aligned}\right\} \tag{3.2}$$

We also require that disturbances vanish far from the interface. The deflection in the interface H is connected to the value of C at $z = 0$ through a linearized version of the boundary condition (2.6) as follows:

$$H = \frac{C(0)}{1 - M^{-1} - q^2\Gamma}. \tag{3.3}$$

Solutions to this system have been computed numerically using the software package SUPORT (Scott & Watts 1977) to solve the two-point boundary-value problem with a secant method to locate the eigenvalues σ.

Our goal in this section is to classify the various normal modes with respect to their dominant physical characteristics. This is most easily achieved by examining the asymptotic behaviour of the modes in a limit of interest. Since the solutal Rayleigh numbers R in typical experiments for binary alloys solidified at rates on the order of microns per second are commonly between 10^6 and 10^7, we choose to examine the asymptotic behaviour of the solutions to (3.1)–(3.2) in the large Rayleigh number limit.

We assume that the quantities q, k, Γ, M, and S are all $O(1)$ parameters as $R \to \infty$ and seek every possible distinguished limit. These are found by rescaling σ, Ψ, and derivatives D on the powers of R that are selected through a balance of appropriate terms in (3.1). There are only three such distinguished limits.

3.1. *Internal waves*

An inviscid fluid with a stable density stratification supports internal-wave motion (Turner 1973). The mechanism of this motion is easily understood: when a parcel of fluid is moved a small distance Δz upward from an initial position z_0 it feels a downward restoring force due to its negative buoyancy equal to $g(\partial\rho_0/\partial z)\Delta z$. The ensuing motion oscillates at the Brunt–Väisälä frequency $N = (-g(\partial\rho_0/\partial z)/\rho_0)^{1/2}$.

The linearized equation of state and the basic-state solute profile lead to a stable density stratification in the liquid ahead of the front. The modes associated with the first distinguished limit correspond to internal waves propagating throughout the solute boundary layer. The first distinguished limit requires $\sigma = O(R^{1/2})$, $\Psi = O(R^{1/2})$, and $\mathrm{D} = O(1)$ as $R \to \infty$ so that these modes have a vertical length scale of the same size as the basic-state profile and a frequency of $O(R^{1/2})$. The connection to internal waves is clear since the Brunt–Väisälä frequency made dimensionless on our time scale of $\mathscr{D}/V^2$ is found to be $N = S^{1/2}R^{1/2}e^{-z/2}$. The frequencies of the first distinguished modes are the frequencies of internal-wave motion.

The leading-order behaviour of the mode as $R \to \infty$ is given by

$$C \sim C_0 + \cdots, \quad \Psi \sim R^{1/2}\Psi_0 + \cdots, \quad \sigma \sim R^{1/2}\sigma_0 + \cdots, \tag{3.4}$$

where

$$S^{-1}\sigma_0(\mathrm{D}^2 - q^2)\Psi_0 + \mathrm{i}qC_0 = 0, \quad \mathrm{i}q\mathrm{e}^{-z}\Psi_0 - \sigma_0 C_0 = 0, \tag{3.5}$$

on $0 \leqslant z < \infty$. These equations are the same as those which govern inviscid internal-wave motion in an isothermal atmosphere and they have the exact solutions

$$\left.\begin{aligned} \Psi_0 = AJ_{2q}(2\mathrm{i}qS^{1/2}\mathrm{e}^{-z/2}/\sigma_0) + BY_{2q}(2\mathrm{i}qS^{1/2}\mathrm{e}^{-z/2}/\sigma_0), \\ C_0 = \mathrm{i}q\mathrm{e}^{-z}\Psi_0/\sigma_0, \end{aligned}\right\} \tag{3.6}$$

where A and B are arbitrary constants and J_ν and Y_ν are the Bessel functions of order ν. The boundary condition that Ψ_0 tends to zero as z tends toward infinity requires that $B = 0$. The remaining boundary conditions are that C_0, Ψ_0, and $\mathrm{D}\Psi_0$ are all zero at the crystal interface. Unfortunately solutions of the form (3.6) cannot be chosen so that these three conditions are simultaneously met. We must choose to impose either the inviscid boundary conditions, $C_0(0) = \Psi_0(0) = 0$, or the viscous no-slip boundary condition $\mathrm{D}\Psi_0(0) = 0$. Both conditions cannot be satisfied.

This apparent overabundance of boundary conditions is caused by a non-uniformity in the asymptotic expansion (3.4) which breaks down as z approaches zero. The manner in which this expansion breaks down is understood – it is well-known that high-frequency oscillatory flows in real fluids develop viscous Stokes layers near boundaries. If ω is the frequency of the outer flow, the scale for the thickness of the Stokes layer is $(\nu/\omega)^{1/2}$. In our case the frequency of the outer flow is proportional to $R^{1/2}$ so that the nearly inviscid internal waves governed by (3.5) blend into a viscous Stokes layer of thickness $R^{-1/4}$ at the solid–liquid interface.

The appropriate boundary conditions which apply to equation (3.5) can be determined via the method of matched asymptotic expansions (Kevorkian & Cole 1981). The structure of the solution near the interface is found by first rescaling vertical lengths on $R^{-1/4}$, introducing the inner variable $\zeta = R^{1/4}z$, and then developing both Ψ and C in an inner expansion,

$$C \sim \hat{C}_0 + R^{-1/4}\hat{C}_1 + \cdots, \quad \Psi \sim R^{1/2}\hat{\Psi}_0 + R^{1/4}\hat{\Psi}_1 + \cdots, \tag{3.7}$$

that must be matched to the outer expansion (3.4) at the edge of the Stokes layer. After rescaling the problem (3.1)–(3.2) using D_* to represent differentiation with respect to ζ, and after introducing the expansion (3.7) we find at leading order that we must evaluate the system

$$\mathrm{D}_*^4\hat{\Psi}_0 - S^{-1}\sigma_0\mathrm{D}_*^2\hat{\Psi}_0 = 0, \quad \mathrm{i}q\hat{\Psi}_0 - \sigma_0\hat{C}_0 + \mathrm{D}_*^2\hat{C}_0 = 0, \tag{3.8}$$

on $0 \leqslant \zeta < \infty$ subject to the boundary conditions at $\zeta = 0$,

$$\hat{\Psi}_0 = \mathrm{D}_*\hat{\Psi}_0 = 0, \quad \hat{C}_0 = 0, \tag{3.9}$$

and the matching condition,

$$\lim_{R\to\infty}\{\Psi(R^{-1/4}\eta\zeta^*) - \hat{\Psi}(\eta\zeta^*)\} = 0, \tag{3.10}$$

where ζ^* is fixed while $\lim_{R\to\infty}\eta = \infty$ and $\lim_{R\to\infty}R^{-1/4}\eta = 0$. It is found that (i) the only leading-order inner solution which satisfies these constraints is $\hat{C}_0(\zeta) = \hat{\Psi}_0(\zeta) = 0$ and (ii) that the matching condition requires the leading-order outer solution to satisfy the inviscid boundary conditions $C_0(0) = \Psi_0(0) = 0$.

If we apply the inviscid conditions to (3.6) we find that the leading-order dispersion relation is selected to be

$$\sigma_0^{(n)} = 2\mathrm{i}qS^{1/2}/\gamma_n, \tag{3.11}$$

where γ_n is real and satisfies $J_{2q}(\gamma_n) = 0$. For each wavenumber q there is a discrete set of modes indexed by n, the number of cells in the vertical direction.

The dispersion relation (3.11) does not indicate whether the internal waves grow or decay in time. To determine the stability of these modes the next correction in σ must be obtained by including higher-order terms in our expansion. The presence of a Stokes layer requires that the outer expansion proceed in powers of $R^{-1/4}$ as follows:

$$\left.\begin{aligned} C \sim C_0 + R^{-1/4}C_1 + \cdots, \quad \Psi \sim R^{1/2}\Psi_0 + R^{-1/4}\Psi_1 + \cdots, \\ \sigma^{(n)} \sim R^{1/2}\sigma_0^{(n)} + R^{1/4}\sigma_1^{(n)} + \cdots. \end{aligned}\right\} \tag{3.12}$$

To calculate the correction in the dispersion relation at next order we must solve the system

$$\left.\begin{aligned} S^{-1}\sigma_0^{(n)}(\mathrm{D}^2 - q^2)\Psi_1 + \mathrm{i}qC_1 = -S^{-1}\sigma_1^{(n)}(\mathrm{D}^2 - q^2)\Psi_0, \\ \mathrm{i}q\mathrm{e}^{-z}\Psi_1 - \sigma_0^{(n)}C_1 = \sigma_1^{(n)}C_0, \end{aligned}\right\} \tag{3.13}$$

subject to boundary conditions. One of the boundary conditions at this order is that Ψ_1 and C_1 tend to zero as z tends toward infinity. The boundary condition at $z = 0$ requires a further examination of the Stokes layer.

At next order in the inner expansion for the Stokes layer we must again solve the system (3.8) for $\hat{C}_1$ and $\hat{\Psi}_1$ subject to the same boundary conditions (3.9) and the same matching condition (3.10). At this order there are non-trivial solutions exhibiting the oscillatory decay in ζ that is characteristic of a Stokes layer. The matching condition now requires that the next-order term in the outer expansion satisfy the *effective* boundary conditions,

$$\Psi_1(0) = -(S/\sigma_0^{(n)})^{1/2}\mathrm{D}\Psi_0(0), \quad C_1(0) = -(S/\sigma_0^{(n)})^{1/2}\mathrm{D}C_0(0), \tag{3.14}$$

where $\mathrm{Re}\,(S/\sigma_0^{(n)})^{1/2} > 0$.

The linear equation (3.13) with the condition of decay at infinity and the boundary conditions (3.14) is inhomogeneous. Because the homogeneous version of this problem has the non-zero solution (Ψ_0, C_0) a solution to the inhomogeneous problem exists only if a solvability condition is satisfied. This condition, which can be determined in a variety of ways, requires $\sigma_1^{(n)}$ to satisfy

$$\sigma_1^{(n)} = -(q^{1/2}S^{3/4}\mathrm{e}^{\pi\mathrm{i}/4})/(2^{1/2}\gamma_n^{1/2}F_q^n), \tag{3.15}$$

where the function $F_q^n = \int_0^\infty \mathrm{e}^{-z}[J_{2q}(\gamma_n\mathrm{e}^{-z/2})]^2\mathrm{d}z/[J'_{2q}(\gamma_n\mathrm{e}^{-z/2})]^2 > 0$.

The correction to the dispersion relation reveals that internal waves are always damped. The time scale of decay is $O(R^{-1/4})$ and for typical directional solidification experiments it is approximately equal to 0.1 s. At first glance it may not appear surprising that the stably stratified liquid is stable but it must be remembered that solidification is occurring and that the solid–liquid interface is deformable. None of the parameters k, Γ, or M appear in the decay rate (3.15) which implies that solidification does not influence the stability of internal waves when Rayleigh numbers are large. Although there is some deformation of the interface associated with these modes, the deformation is slight. It follows directly from the relation (3.3) and the expansion (3.12) that the interface deformation satisfies $H = O(R^{-1/4})$. Although these internal waves are stable, they may be driven to instability by the presence of externally imposed vibration (Brattkus 1992). The effects of external vibration have also been studied in the statically stable case by Wheeler *et al.* (1991).

3.2. *Buoyancy edge waves*

Another class of modes is associated with the second possible distinguished limit requiring $\sigma = O(R^{1/3})$, $\Psi = O(R^{1/3})$, and $\mathrm{D} = O(R^{1/6})$ as $R \to \infty$. We label this second class of modes 'buoyancy edge waves' since they are convective modes confined to a layer near the interface of thickness $O(R^{-1/6})$.

These modes are essentially trapped internal waves. As the index n which measures the number of vertical cells in an internal-wave mode increases, the thickness δ_p of the primary cell closest to the interface decreases. The stream function (3.5) can be used to show that $\delta_p \sim 2/n$. At the same time, because the frequency of the internal wave decreases as n increases, the thickness of the Stokes layer δ_s increases as $\delta_s \sim n^{1/2}R^{-1/4}$. The scalings in the second distinguished limit are precisely those which correspond to values of n where the Stokes layer and the primary cell overlap, $\delta_p \sim \delta_s$. In this sense the second class of modes may be viewed as an internal wave trapped at the interface by viscosity.

For the buoyancy edge waves we have

$$\left.\begin{aligned} C \sim C_0 + R^{-1/6}C_1 + \cdots, \quad \Psi \sim R^{1/3}\Psi_0 + R^{1/6}\Psi_1 + \cdots, \\ \sigma \sim R^{1/3}\sigma_0 + R^{1/6}\sigma_1 + \cdots, \end{aligned}\right\} \tag{3.16}$$

as $R \to \infty$ where the leading-order system,

$$\mathrm{D}_*^4\Psi_0 - S^{-1}\sigma_0\mathrm{D}_*^2\Psi_0 - \mathrm{i}qC_0 = 0, \quad \mathrm{i}q\Psi_0 + \mathrm{D}_*^2C_0 - \sigma_0C_0 = 0, \tag{3.17}$$

on $0 \leqslant \zeta < \infty$ is subject to the boundary conditions at $\zeta = 0$,

$$\Psi_0 = \mathrm{D}_*\Psi_0 = 0, \quad C_0 = 0. \tag{3.18}$$

The vertical coordinate has been rescaled here to be $\zeta = R^{1/6}z$. Although it is a simple enough matter to extract from this system a characteristic equation for σ_0, the characteristic equation is awkward to analyse. We adopt a different tack and determine that all of these modes are stable by proving indirectly that $\mathrm{Re}\,\sigma_0 < 0$. To show this we notice that the equation

$$\int_0^\infty \left[\Psi_0^*\mathrm{D}_*^2(\mathrm{D}_*^2 - S^{-1}\sigma_0)\Psi_0 - C_0^*(\mathrm{D}_*^2 - \sigma_0)C_0\right]\mathrm{d}\zeta = 2\mathrm{i}q\int_0^\infty \mathrm{Re}\,\Psi_0^*C_0\mathrm{d}\zeta, \tag{3.19}$$

follows directly from (3.17) where superscript asterisks denote complex conjugation. If we integrate the left-hand side of this expression by parts we find that

$$\mathrm{Re}\,\sigma_0\int_0^\infty \left[|C_0|^2 + S^{-1}|\mathrm{D}_*\Psi_0|^2\right]\mathrm{d}\zeta = -\int_0^\infty \left[|\mathrm{D}_*^2\Psi_0|^2 + |\mathrm{D}_*C_0|^2\right]\mathrm{d}\zeta. \tag{3.20}$$

It is clear from (3.20) that $\mathrm{Re}\,\sigma_0 < 0$ and that the inequality is strict since if $\mathrm{Re}\,\sigma_0 = 0$ it is necessary that both Ψ_0 and C_0 be identically zero.

This second class of modes is always stable and the buoyancy edge waves decay on a time scale which is asymptotically faster than the scale of decay for internal waves. It follows from (3.3) that the interface deflection for these modes satisfies $H = O(R^{-1/6})$, larger than the deflection found for the internal waves but still asymptotically small.

3.3. *The Mullins–Sekerka mode*

In the absence of convection a directional solidification front is subject to morphological instabilities. The original linear stability analysis of Mullins & Sekerka (1964) demonstrated that planar growth is unstable whenever the parameter M exceeds a critical value M_c. They also predicted the critical wavenumber q_c of the first unstable

mode. This instability is present in the system (3.1)–(3.2) when both the solutal Rayleigh number R and the stream function Ψ are set to zero.

The morphological instability persists when $R > 0$ although the horizontal concentration variations associated with the instability now produce a baroclinically driven convection (Coriell *et al.* 1980; Hurle *et al.* 1982). The horizontal variation in concentration near the interface is given by (3.3), $C(0)e^{iqx} = (1 - M^{-1} + \Gamma q^2)He^{iqx}$. From this expression it is clear that the perturbed concentration is largest at crests in the interface and that in these regions the fluid mixture is densest. This variation in density produces a torque on the fluid and causes fluid to be convected from the crests toward depressions in the interface. Because the added solute that is transported with the fluid tends to reduce the temperature of the interface in accordance with thermodynamic equilibrium, the result of this flow is that it tends to melt back or deepen interfacial depressions. As a result, buoyancy effectively destabilizes the interface, reducing the value of M_c as R increases.

The extent to which convection destabilizes the morphological instability depends on the wavenumber q. The trend of this dependence is suggested by examining the unstable mode when $R = 0$. If R and Ψ are set to zero the eigenfunction of system (3.1)–(3.2) is $e^{iqx+\sigma t-\frac{1}{2}[1+(1+4(\sigma+q^2))^{1/2}]z}$. As q increases, this disturbance is confined to a progressively thinner layer near the crystal interface. When R is small but nonzero the convection driven by this concentration distribution is also confined to a progressively thinner layer at the interface as q increases. Since it seems reasonable to conjecture that convection localized at the interface is less effective in transporting solute along the interface, we expect the destabilizing effects of convection to be reduced as q increases. The most significant destabilization due to solute buoyancy should occur for long-wavelength disturbances. Because of this trend one expects the critical wavenumber q_c to be shifted toward smaller values as R increases.

The last distinguished limit as $R \to \infty$ is a Mullins–Sekerka mode which, unlike the previous two modes, is accompanied by a significant deformation of the interface. The mode is characterized by the scalings $\sigma = O(R^{1/6}), \Psi = O(R^{1/3}), \mathrm{D} = O(R^{1/6})$. After the vertical coordinate $\zeta = R^{1/6}z$ is introduced, the asymptotic expansion of this third class of modes proceeds in powers of $R^{-1/6}$,

$$\left.\begin{aligned} C \sim C_0 + R^{-1/6}C_1 + \cdots, \quad \Psi \sim R^{1/3}\Psi_0 + R^{1/6}\Psi_1 + \cdots, \\ \sigma \sim R^{1/6}\sigma_0 + \sigma_1 + \cdots, \end{aligned}\right\} \tag{3.21}$$

as $R \to \infty$. The equations governing the leading-order terms become

$$\mathrm{D}_*^4\Psi_0 - iqC_0 = 0, \quad iq\Psi_0 + \mathrm{D}_*^2C_0 = 0, \tag{3.22}$$

and they are subject to the boundary conditions at $\zeta = 0$,

$$\Psi_0 = \mathrm{D}_*\Psi_0 = 0, \quad (1 - M^{-1} - \Gamma q^2)\mathrm{D}_*C_0 + \sigma_0 C_0 = 0, \tag{3.23}$$

and a condition of decay at infinity.

The eigenfunctions of this system are exponential functions of the variable $q^{1/3}\zeta$:

$$\begin{aligned} \Psi_0 &= (1+\alpha_2)e^{\alpha_1|q|^{1/3}\zeta} + (\alpha_1 - \alpha_2)e^{-|q|^{1/3}\zeta} - (1+\alpha_1)e^{\alpha_2|q|^{1/3}\zeta}, \\ C_0 &= -i|q|^{1/3}[(1+\alpha_1)e^{\alpha_1|q|^{1/3}\zeta} + (\alpha_1 - \alpha_2)e^{-|q|^{1/3}\zeta} - (1+\alpha_2)e^{\alpha_2|q|^{1/3}\zeta}], \end{aligned} \tag{3.24}$$

where $\alpha_j = e^{2\pi ij/3}$ and the characteristic equation for σ_0 is simply

$$\sigma_0 = \tfrac{1}{2}(1 - M^{-1} - \Gamma q^2)|q|^{1/3}. \tag{3.25}$$

The unstable eigenfunctions are presented graphically in figure 2. Growth rates

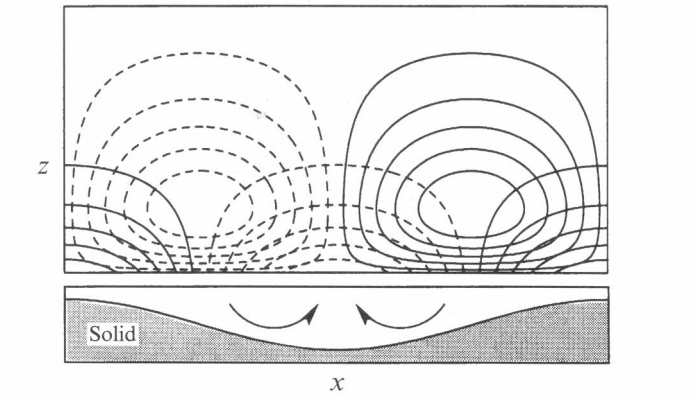

FIGURE 2. The interface shape, isopycnals, and streamlines for perturbations described by the eigenfunction (3.24). The interface at $z = 0$, with its depression in the centre of the figure, is enlarged and displayed in the lower box. The closed curves are streamlines and the curves which intersect the interface are lines of constant solute concentration. Dashed curves correspond to negative values: the liquid is depleted of solute and is rising above depressions in the interface.

are positive and the interface is morphologically unstable when $M > 1$ and the critical wavenumber at this order in the approximation is zero. As we expected, the morphological instability is a long-wavelength instability for large Rayleigh numbers. Even though the surface-energy parameter is non-zero, buoyancy has destabilized the morphological instability to the level of the constitutional undercooling criterion.

When $q = 0$ in the original linear problem (3.1)–(3.2), convection decouples from the diffusion of solute and it has been noted previously that without non-equilibrium effects the Mullins–Sekerka mode is stable to pulsatile motion (Merchant & Davis 1990). The conclusion that $q = 0$ is the critical wavenumber must be incorrect. The source of the problem here is that the expansion (3.21) is not uniform for all values of q. It can be shown that although the expansion is valid for $q^2R \gg 1$, it breaks down as q tends to zero. A higher-order approximation for the growth rate σ is required to find the correct critical wavenumber. The correction term σ_1 is found by proceeding to next order where we must solve the system

$$\left.\begin{aligned} \mathrm{D}_*^4\Psi_1 - \mathrm{i}qC_1 &= -S^{-1}\mathrm{D}_*^2(\mathrm{D}_* - \sigma_0)\Psi_0, \\ \mathrm{i}q\Psi_1 + \mathrm{D}_*^2C_1 &= \mathrm{i}q\zeta\Psi_0 - (\mathrm{D}_* - \sigma_0)C_0, \end{aligned}\right\} \tag{3.26}$$

subject to the boundary conditions at $\zeta = 0$,

$$\left.\begin{aligned} \Psi_1 = \mathrm{D}_*\Psi_1 &= 0, \\ (1 - M^{-1} - \Gamma q^2)\mathrm{D}_*C_1 + \sigma_0 C_1 &= [(1-k)(M^{-1} + \Gamma q^2) - \sigma_1 - 1]C_0, \end{aligned}\right\} \tag{3.27}$$

and decay at infinity. The system (3.26)–(3.27) is inhomogeneous and has a non-zero homogeneous solution corresponding to the leading-order eigenfunctions Ψ_0 and C_0. There is a solution to the system only if an appropriate compatibility condition is satisfied. The condition in this case requires

$$\sigma_1 = -k + (k - \tfrac{7}{12})(1 - M^{-1} - \Gamma q^2) + \tfrac{1}{48}(17 - S^{-1})(1 - M^{-1} - \Gamma q^2)^2. \tag{3.28}$$

The asymptotic approximation for the growth rate σ, valid to $O(R^{-1/6})$, is

$$\sigma \sim \tfrac{1}{2}(1 - M^{-1} - \Gamma q^2)(q^2R)^{1/6} - k + (k - \tfrac{7}{12})(1 - M^{-1} - \Gamma q^2) + \tfrac{1}{48}(17 - S^{-1})(1 - M^{-1} - \Gamma q^2)^2, \tag{3.29}$$

C_∞ (% wt)	G (K cm^{-1})	V (μm s^{-1})	R	σ_a	σ_n
2.5	125.0	5.0	8.5×10^4	2.461	2.544
1.0	20.0	2.0	5.3×10^5	3.432	3.492
0.5	5.0	1.0	2.1×10^6	4.384	4.432

TABLE 1. A comparison of the growth rate σ_n numerically computed from (3.1)–(3.2) *vs.* the asymptotic value σ_a predicted by equation (3.29). Three experimental conditions are listed. Using the material parameters appropriate for a Sn-Pb alloy these correspond to fixing the parameters $q = 1, k = 0.12, S = 120, M = 5.6, \Gamma = 7.3 \times 10^{-6}$. The asymptotic result approaches the numerical result as the solutal Rayleigh number R increases. Growth rates increase with Rayleigh number, i.e. buoyancy destabilizes the morphological instability.

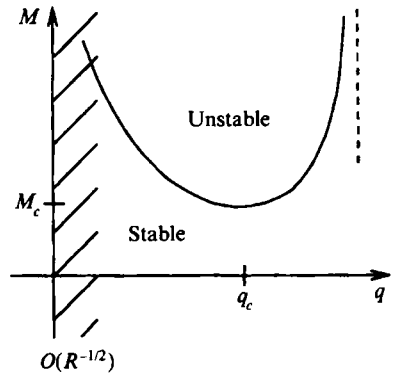

FIGURE 3. A schematic of the marginal stability curve for morphological modes at large Rayleigh numbers. In the hatched region near $q = 0$ the two-termed asymptotic approximation given by equation (3.29) is not valid. All wavenumbers to the right of the dashed line located near $q = \Gamma^{-1/2}$ are absolutely stable.

as $R \to \infty$. This result is confirmed in table 1 through a comparison between the growth rates given by the expression above and those computed numerically from the full system (3.1)–(3.2). Rayleigh numbers must be relatively large before the comparison becomes accurate. We can use (3.29) to determine a more refined estimate of the critical wavenumber q_c for the morphological instability.

The marginal stability curve divides the (M, q)-plane into regions of stability and instability. The critical pair (M_c, q_c) is the lowest point along this curve. When the two principal terms are retained in (3.29) near the marginal stability curve, the growth rate is approximately described by

$$\sigma \sim \tfrac{1}{2}(1 - M^{-1} - \Gamma q^2)(q^2 R)^{1/6} - k \quad \text{as} \quad R \to \infty, \tag{3.30}$$

which leads to the marginal stability relation $\frac{1}{2}(1 - M^{-1} - \Gamma q^2)(q^2 R)^{1/6} \sim k$. If this result is used to compute the critical data we find that

$$M_c \sim 1 + \tfrac{7}{3}(3\Gamma k^6)^{1/7} R^{-1/7}, \quad q_c \sim (3\Gamma/k)^{-3/7} R^{-1/14}. \tag{3.31}$$

The two-term approximation to the growth rate predicts a critical wavenumber that satisfies the restriction $q^2 R \gg 1$ and therefore lies within the range where (3.29) is asymptotically valid. A schematic of the marginal stability curve appears in figure 3.

4. Morphological instabilities; nonlinear theory

The linear theory developed in the previous section can be used to determine the dominant scales at transition. For large values of the Rayleigh number, linear theory predicts that a transition from planar to non-planar interfaces occurs when M is slightly above unity and that the horizontal scale of the transition is set by the wavelength of the unstable mode, $\lambda_c = 2\pi/q_c = O(R^{1/14})$. Since the eigenfunctions depend on $q^{1/3}\zeta$, the appropriate vertical length scale at transition is $q_c^{-1/3}R^{-1/6} = O(R^{-1/7})$. The expression for the growth rate (3.29) near critical reveals that the relevant time scale for the dynamics of the transition is $O(1)$ as $R \to \infty$.

We build these scalings derived from linear theory directly into the *nonlinear* problem (2.2),(2.4)–(2.6) by defining the following variables:

$$X = R^{-1/14}x, \quad Z = R^{1/7}z, \quad T = t, \quad \mu = (1 - M^{-1})R^{1/7}, \tag{4.1}$$

and expanding the solution to the nonlinear problem in an asymptotic series as $R \to \infty$. The information needed to develop this asymptotic series is not completely contained in the linear theory. For example, linear theory predicts the ratio of the leading-order scales for the linearized concentration and the stream function but it does not indicate the size of the concentration deviations as compared to the basic-state exponential profile. Similarly, linear theory does not predict the size of the deflection in the interface. The magnitude of the first correction to the basic state and the size of the interface deflection are chosen in our expansion so that nonlinear terms are promoted to leading-order in the asymptotic theory. This criterion requires the following expansions:

$$\left.\begin{aligned} c &= \mathrm{e}^{-R^{-1/7}Z} + R^{-2/7}C_0(X,Z,T) + \cdots, \\ \psi &= R^{1/14}\Psi_0(X,Z,T) + \cdots, \\ h &= R^{-1/7}H(X,T) = R^{-1/7}H_0(X,T) + \cdots. \end{aligned}\right\} \tag{4.2}$$

Since the scale on the interface h is the same as the vertical scale, the interface in the new coordinates is located at $Z = H$ where H is not necessarily small.

Inserting these scalings into the governing equations (2.2),(2.4)–(2.6) and collecting the leading-order terms in $R^{-1/14}$ we find the following system:

$$\Psi_{0ZZZZ} - C_{0X} + H_{0X}C_{0Z} = 0, \quad \Psi_{0X} + C_{0ZZ} - H_{0X}\Psi_{0Z} = 0, \tag{4.3}$$

which is subject to the boundary conditions applied at $Z = 0$,

$$\left.\begin{aligned} \Psi_0 = \Psi_{0Z} = 0, \quad C_{0Z} + kH_0 + H_{0T} = 0, \\ C_0 = \mu H_0 - \tfrac{1}{2}H_0^2 + \Gamma H_{0XX}, \end{aligned}\right\} \tag{4.4}$$

and a condition that both C_0 and Ψ_0 approach zero far from the interface. The reduced system (4.3)–(4.4) is quasi-steady (time derivatives appear only in the boundary conditions) and a coordinate translation, $Z \mapsto Z + H$, has been introduced so that the location of the interface is fixed at $Z = 0$.

The problem described above is a free-boundary problem for the leading-order position of the interface H_0. The common development of a long-wave theory leads to one-dimensional fields at leading order and an evolution equation for the interface at higher orders (Riley & Davis 1990). Here the leading-order theory is two-dimensional and does not immediately lead to an evolution equation for the interface H_0. Although the reduced system is a significant simplification over the original nonlinear problem (2.2),(2.4)–(2.6), the further reduction to an evolution equation for the interface is important. Numerical solutions are more easily obtained from an

evolution equation and simulations on a three-dimensional version of the reduced system currently require it.

We can reduce the system to a single evolution equation by first obtaining the matrix Green's function $\mathbf{G}(p|p')$ that satisfies the following 2×2 system of equations

$$(\boldsymbol{L} - H_{0X}\boldsymbol{M})\mathbf{G}(p|p') = \delta(p - p')\boldsymbol{I} \tag{4.5}$$

where $\boldsymbol{L} - H_{0X}\boldsymbol{M}$ is shorthand for the operator appearing in equation (4.3) (for example $L^{(11)}$ represents $\partial^4/\partial Z^4$). Here $p = (X, Z)$ and $\delta(p - p')$ is a delta function with its source at p'. The Green's function decays as Z tends to infinity and $\mathbf{G}$ satisfies the conditions

$$G^{(11)}(p_0|p') = G^{(12)}(p_0|p') = 0, \quad \mathbf{G}_Z(p_0|p') = 0, \tag{4.6}$$

along the boundary $p_0 = (X, 0)$. Once this Green's function is determined it can be used to show that H_0 must satisfy the following evolution equation:

$$\mu H_0 - \tfrac{1}{2}H_0^2 + \Gamma H_{0XX} + \int_{-\infty}^{\infty} K(X, X')[kH_0 + H_{0T}]\mathrm{d}X' = 0, \tag{4.7}$$

where the kernel K is related to the Green's function through $K(X, X') = 2G^{(22)}(p_0|p')$. The kernel depends implicitly on H_0; the evolution equation is *nonlocal* and *nonlinear*.

Although it is difficult to determine a closed-form expression for the Green's function, a Neumann series for $\mathbf{G}(p|p')$ can be constructed by iterating the equation (4.5). In this way the Green's function may be represented by the series

$$\mathbf{G}(p|p') = \mathbf{G}_0(p|p') + \mathbf{G}_1(p|p') + \mathbf{G}_2(p|p') + \cdots, \tag{4.8}$$

where

$$\mathbf{G}_{i+1}(p|p') = \int_0^{\infty}\int_{-\infty}^{\infty} \mathbf{G}_0(p|p'')H_{0X}\boldsymbol{M}\mathbf{G}_i(p''|p')\mathrm{d}p'', \quad i = 0, 1, 2, \ldots \tag{4.9}$$

and $\mathbf{G}_0(p|p')$ satisfies $\boldsymbol{L}\mathbf{G}_0(p|p') = \delta(p - p')\boldsymbol{I}$ with the boundary conditions (4.6). We have solved for the first term in the Neumann series expansion of the Green's function and determined that

$$K_0(X, X') = 2G_0^{(22)}(p_0|p') = \Gamma(2/3)|X - X'|^{-2/3}/\pi. \tag{4.10}$$

where $\Gamma(\cdot)$ is not the surface energy here but the Gamma function. This first term is sufficient to analyse the linear stability of a planar solution $H_0 = 0$ directly from the evolution equation; the resulting linear theory reclaims the dispersion relation (3.30). When the interfacial slopes H_{0X} are bounded the Neumann series (4.8) is expected to converge rapidly; the evolution equation (4.7) should serve as the starting point for an efficient numerical simulation of the interface.

5. Non-planar solidification

The long-wave theory outlined above represents an asymptotic reduction of the governing system (2.2),(2.4)–(2.6) for large Rayleigh numbers which significantly simplifies the discussion of morphological instabilities. For example, the Landau equation describing the nonlinear development of the amplitude for the most unstable mode near transition can be determined analytically from (4.3),(4.4) while numerics are required to determine the same equation from the original system.

In this section we use the long-wave theory to search for *steady, non-planar* solutions to the directional solidification problem. The task is simplified by seeking self-similar solutions to (4.3), (4.4) which exist only if two additional provisions are adopted. First,

similarity solutions exist only if the surface-energy parameter Γ is zero. Although Γ is typically quite small, the limit $\Gamma \to 0$ in equation (4.6) is a singular limit which requires attention. We assume here that Γ is identically zero. A second provision, sufficient for self-similarity, is that the physical constant μ is proportional to the local temperature (or equivalently to the vertical coordinate z). Because we have treated all of the parameters that appear in the definition of μ as constant, this second allowance is seemingly of dubious physical consequence except in the case where the proportionality constant is zero, that is where $M = 1$. For the moment we assume μ is proportional to z. The proportionality constant $\hat{\mu}$ will be viewed as a non-physical continuation parameter that allows us to calculate non-planar solutions at a physically meaningful value of $\hat{\mu} = 0$.

We introduce the similarity variable $\eta = Z|X|^{-1/3}$ and define

$$\Psi_0 = X\Psi(\eta), \quad C_0 = |X|^{2/3}C(\eta), \quad H_0 = |X|^{1/3}H, \quad \mu = |X|^{1/3}\hat{\mu}, \tag{5.1}$$

so that (4.3) becomes a system of ordinary differential equations for Ψ and C,

$$\Psi'''' + \tfrac{1}{3}(H+\eta)C' - \tfrac{2}{3}C = 0, \quad C'' - \tfrac{1}{3}(H+\eta)\Psi' + \Psi = 0, \tag{5.2}$$

on $0 \leqslant \eta < \infty$, subject to the boundary conditions at $\eta = 0$,

$$\Psi = \Psi' = 0, \quad C' + kH = 0, \quad C = \hat{\mu}H - \tfrac{1}{2}H^2, \tag{5.3}$$

and a condition of decay as $\eta \to \infty$. Primes denote differentiation with respect to the similarity variable η. The system above is an eigenvalue problem for the interface 'shape', H.

A numerical integration of the differential equations (5.2) reveals a strong tendency for solutions to develop algebraic growth in η. When zero conditions are imposed at the right end of a large but finite interval, a spurious boundary layer develops. This layer is inconsistent with the conditions of decay we require. Fortunately, the interior growth can be eliminated by observing that there are two exact solutions to the differential equations: $C = 0, \Psi = (H+\eta)^3$ and $C = (H+\eta)^2, \Psi = -2$. The first exact solution corresponds to a far-field shear flow with horizontal velocities scaling on Z^2. The second exact solution corresponds to a constant vertical flow. Since we are interested in the case of no far-field flow, neither of these solutions is allowed. We can use these solutions to reduce the order of the system and to eliminate the difficulty with spurious boundary layers. These solutions can be eliminated through the substitution

$$\Psi' = \begin{cases} 3(H+\eta)^2 \displaystyle\int_0^\eta (H+x)^{-3}\phi(x)\mathrm{d}x, & 0 \leqslant \eta < 1, \\ -3(H+\eta)^2 \displaystyle\int_\eta^\infty (H+x)^{-3}\phi(x)\mathrm{d}x, & 1 < \eta \leqslant \infty, \end{cases} \tag{5.4}$$

where ϕ must satisfy the differential equation,

$$(H+\eta)^2\phi'''' - 2(H+\eta)\phi''' + 2\phi'' + \tfrac{1}{9}(H+\eta)^4\phi = 0, \tag{5.5}$$

with the boundary conditions at $\eta = 0$,

$$\phi'' = \tfrac{2}{9}\hat{\mu}H^2 - \tfrac{1}{9}(1-k)H^3, \quad H\phi''' - \phi'' = -\tfrac{k}{9}H^3. \tag{5.6}$$

An auxiliary condition,

$$\int_0^\infty \phi(x)\mathrm{d}x = 0, \tag{5.7}$$

guarantees that $\Psi(0) = 0$.

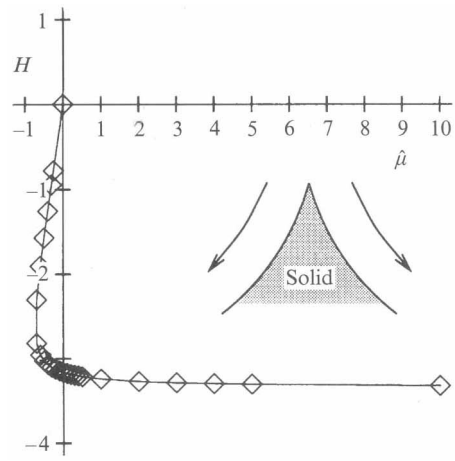

FIGURE 4. Computed values for the eigenvalue H of the system (5.5-5.7) as a function of the continuation parameter $\hat{\mu}$ when $k = 0.12$. The similarity solutions branch from the planar solution, $H = 0$, subcritically to negative values of $\hat{\mu}$. The branch turns around and solutions move into the supercritical range. There are two solutions when $\hat{\mu} = 0$: the planar front and a non-planar front with $H \doteq -3.16$

When $H > 0$ SUPORT has no difficulty in solving the boundary-value problem (5.5)–(5.6). No solutions satisfying the auxiliary condition $\int_0^\infty \phi(x)\mathrm{d}x = 0$ are found.

When $H < 0$ the differential equation has a regular singular point at $\eta = -H$. The form of the substitution (5.4) was chosen so that all solutions to (5.5) are analytic at the singular point; this is revealed through a local analysis of ϕ near $\eta = -H$. Even though a local analysis of ϕ near the singular point reveals that all solutions are analytic there, some care must be taken when numerically integrating through this point. To integrate the equation when $H < 0$ we first make H complex to move the singularity off the integration path. If $\mathrm{Im}\, H$ is fixed and sufficiently large, the system can be integrated without difficulty. Non-zero values of $\mathrm{Re}\, H < 0$ are found such that all of the conditions of the problem (5.5)–(5.7) are satisfied. The value of $\mathrm{Im}\, H$ is then decreased until $\mathrm{Re}\, H$ converges.

The results are shown in figure 4. There is a branch of similarity solutions which emerges from the planar solution $H = 0$ and extends slightly into the subcritical range $\hat{\mu} < 0$ before turning around and continuing on for positive values of $\hat{\mu}$. The fact that similarity solutions exist only for $H < 0$ means that the self-similar solid–liquid interface always bends back toward lower temperatures. The interface has an upward pointing cusp at the origin that separates counter-rotating convection cells. When the self-similar stream function is used to determine the vertical velocity near the front we find that $w \sim 3\eta^2\phi(0)/2H$. The computed values for $\phi(0)$ are always found to be positive when $H < 0$ indicating that fluid is swept from the cusp downward along the interface.

The meaning of the similarity solutions with $\hat{\mu} \neq 0$ is not clear since they require physical constants to vary along the interface. We consider $\hat{\mu}$ to be a non-physical continuation parameter that allows us to compute the non-planar similarity solution in the case when $\hat{\mu} = 0$, a case which is equivalent to fixing the morphological number M to unity everywhere.

6. Summary

There are two principal items of importance in our paper. The first is that thermal buoyancy is not necessary to produce long-wavelength instabilities during upward directional solidification. Because of the preferential destabilization of small wavenumbers, strong solute buoyancy alone is sufficient to increase the wavelength of critical disturbances.

The second item is that the asymptotic theory developed for large solutal Rayleigh numbers exhibits solutions that represent steady, non-planar solidification fronts. We have found a similarity solution at $M = 1$ which bends backward toward lower temperatures. A cusp in the interface separates two counter-rotating convection cells that sweep solute in the melt from the cusp downward along the front. We would like to make an analogy between this non-planar solidification and the observations of steepling in directional solidification experiments. Steepling is observed when a planar array of either dendritic or cellular microstructure suddenly bends backward toward colder temperatures. We have replaced this planar array of microstructure by a flat, sharp interface. The shape of our self-similar non-planar front is not identical to those seen experimentally: for example, (i) a cusp has never been observed on a steepled interface and (ii) the curvature of our front has the opposite sign of those observed. However, the non-planar, macroscopically curved solution captures the essence of the qualitative description of steepling due to Burden *et al.* (1973). Although this 'steepled' interface does not require thermal buoyancy as Coriell & McFadden (1989) suggested, it occurs precisely at the point when the planar front first becomes morphologically unstable, i.e. when $M = 1$. This is consisitent with the suggestion of Coriell & McFadden (1989) that steepling is connected to a morphological instability of planar fronts.

At the moment we do not know whether the similarity solution is stable or whether it persists for non-zero capillarity. Since the curvature of the cusp singularity in the interface of the similarity solution is bounded, the exclusion of surface energy is not expected to significantly modify the solution.

Long-wavelength instabilities in directional solidification are sensitive to our approximation of a linear and imperturbable temperature field (Coriell & McFadden 1993). The long-wave theory developed in this paper is relevant to materials whose solid and liquid phases have equivalent thermal properties with a thermal diffusivity that is much larger than the solute diffusivity. The Stefan number VL_v/KG (L_v is the latent heat of fusion and K is the thermal conductivity) must also be small. Since the materials which actually satisfy these criteria are few, the long-wave theory should be viewed as a qualitative description of a unique morphological instability.

REFERENCES

BRATTKUS, K. 1992 Stimulated convection and morphological instability. In *Interactive Dynamics of Convection and Solidification* (ed. S. H. Davis, H. E. Huppert, U. Müller & M. G. Worster). NATO ASI Series E, vol. 219, pp. 23–25. Kluwer Academic.

BURDEN, M. H., HEBDITCH, D. J. & HUNT, J. D. 1973 Macroscopic stability of a planar, cellular or dendritic interface during directional solidification. *J. Cryst. Growth* **20**, 121–124.

CORIELL, S. R., CORDES, M. R., BOETTINGER, W. S. & SEKERKA, R. F. 1980 Convective and interfacial instabilities during unidirectional solidification of a binary alloy. *J. Cryst. Growth* **49**, 13–28.

CORIELL, S. R. & MCFADDEN, G. B. 1989 Buoyancy effects on morphological instability during directional solidification. *J. Cryst. Growth* **94**, 513–521.

CORIELL, S. R. & MCFADDEN, G. B. 1993 Morphological stability. In *Handbook of Crystal Growth 1. Fundamentals Part B: Transport and Stability* (ed. D. T. J. Hurle), pp. 785–857. North-Holland.

DAVIS, S. H. 1990 Hydrodynamic interactions in directional solidification. *J. Fluid Mech.* **212**, 241–262.

GLICKSMAN, M. E., CORIELL, S. R., & MCFADDEN, G. B. 1986 Interaction of flows with the crystal-melt interface. *Ann. Rev. Fluid Mech.* **18**, 307–335.

HURLE, D. T. J., JAKEMAN, E. & WHEELER, A. A. 1982 Effect of solutal convection on the morphological stability of a binary alloy. *J. Cryst. Growth* **58**, 163–179.

KEVORKIAN, J. & COLE, J. D. 1981 *Perturbation Methods in Applied Mathematics*. Springer.

LANGER, J. S. 1980 Instabilities and pattern formation in crystal growth. *Rev. Mod. Phys.* **52**, 1–28.

MERCHANT, G. J. & DAVIS, S. H. 1990 Morphological instability in rapid directional solidification. *Acta Metall. Mater.* **38**, 2683–2693.

MULLINS, W. W. & SEKERKA, R. F. 1964 Stability of a planar interface during directional solidification of a dilute binary alloy. *J. Appl. Phys.* **35**, 444–451.

RILEY, D. S. & DAVIS, S. H. 1990 Long-wave morphological instabilites in the directional solidification of a dilute binary mixture. *SIAM J. Appl. Maths* **50**, 420–436.

SCOTT, M. R. & WATTS, H. A. 1977 Computational solution of linear two-point boundary value problems via orthonormalization. *SIAM J. Numer. Anal.* **14**, 40–70.

TURNER, J. S. 1973 *Buoyancy Effects in Fluids*. Cambridge University Press.

VERHOEVEN, J. D., MASON, J. T., & TRIVEDI, R. 1986 The effect of convection on the dendrite to eutectic transition. *Metall. Trans.* A **17**, 991–1000.

WHEELER, A. A., MCFADDEN, G. B., MURRAY, B. T. & CORIELL, S. R. 1991 Convective stability in the Rayleigh-Benard and directional solidification problems: high-frequency gravity modulation. *Phys. Fluids* A **3**, 2847–2858.